Electronic Supplementary Information for

Crystal structure engineering of metal halide perovskites for photocatalytic organic synthesis

Chunhua Wang,[a] Yang Ding,[b] Biao Liu,[c] Bo Weng,*[d] Johan Hofkens,*[ae] Maarten B. J. Roeffaers*[d]

[a]Department of Chemistry, KU Leuven, Celestijnenlaan 200F, 3001 Leuven, Belgium.

[b]Laboratory of Inorganic Materials Chemistry (CMI), University of Namur, 61 rue de Bruxelles, B-5000, Namur, Belgium.

[c]Hunan Key Laboratory for Super-microstructure and Ultrafast Process, School of Physics and Electronics, Central South University, Changsha 410083, P. R. China.

[d]cMACS, Department of Microbial and Molecular Systems, KU Leuven, Celestijnenlaan 200F, 3001 Leuven, Belgium.

[e]Max Planck Institute for Polymer Research, Ackermannweg 10, 55128 Mainz, Germany.

*Corresponding authors

Email: maarten.roeffaers@kuleuven.be; johan.hofkens@kuleuven.be; bo.weng@kuleuven.be

Table of Contents

1. Materials and reagents

Bismuth(III) bromide ($BiBr_3$), potassium bromide (KBr), potassium palladium(II) chloride (K_2PdCl_4) and benzyl alcohol (C_6H_5OH) were purchased from Sigma-Aldrich. Benzotrifluoride (BTF) and Dimethyl sulfoxide (DMSO) were purchased from Alfa Aesar. Bismuthiol I (1,3,4-thiadiazole-2,5-dithiol ($C_2H_2N_2S_3$)) was supplied by Fluka. All chemicals were used without further purification.

2. Photocatalyst preparation

2.1 Preparation of $Cs_3Bi_2Br_9$ and Cs_3BiBr_6

$Cs_3Bi_2Br_9$ and Cs_3BiBr_6 materials were synthesized based on an anti-solvent precipitation method at room temperature. CsBr and $BiBr_3$ with a molar ratio of $CsBr/BiBr_3$=3:2 or $CsBr/BiBr_3$=3:1 was dissolved in DMSO at a concentration of 0.15 M to form the $Cs_3Bi_2Br_9$ and Cs_3BiBr_6 precursor solution, respectively. Then, the precursor solution was added to isopropanol to get the $Cs_3Bi_2Br_9$ or Cs_3BiBr_6 suspension. Finally, the products were dried at 60 ^oC in a vacuum oven overnight.

2.2 Synthesis of palladium nanocubes

Palladium nanocubes (Pd NCs) were synthesized based on the reported method.[1] In a typical experiment, 105 mg poly(vinyl pyrrolidone) (PVP), 600 mg potassium bromide (KBr) and 60 mg L-ascorbic acid (AA) were added in an 8 mL deionized water and stirred at 80 ^oC for 10 min. After that, 63 mg K_2PdCl_4 was dissolved in 3 mL deionized and added to the above solution, and the mixture was stirred at 80 ^oC for 3 h. Finally, the product was collected and washed with isopropanol several times before redispersion in the isopropanol solution.

2.3 Synthesis of $Pd/Cs_3Bi_2Br_9$ and Pd/Cs_3BiBr_6 composites

The 1 wt% $Pd/Cs_3Bi_2Br_9$ and 1 wt% Pd/Cs_3BiBr_6 composites were synthesized at room temperature through the above similar precipitation method. In a typical experiment (1% $Pd/Cs_3Bi_2Br_9$ and 1% Pd/Cs_3BiBr_6), 100 mg $Cs_3Bi_2Br_9$ or Cs_3BiBr_6 was first added in 15 mL isopropanol and kept stirring for 20 min. Then, 20 mL of isopropanol solution containing 1 mg Pd was added dropwise into the vigorously stirred $Cs_3Bi_2Br_9$ or Cs_3BiBr_6 suspension and kept stirring at room temperature for 12 h. Finally, the products were collected and dried in a vacuum oven at 60 ^oC.

3. Characterization

3.1 Instrumentations and methods

XRD patterns of the materials were measured using an X-ray diffractometer (Cu Kα1 radiation, λ=1.5406 Å) by scanning the samples in the 2 θ ranging from 10 to 70 degrees at a scan rate of 0.02°/s. Scanning electron micrographs (SEM) were recorded by scanning electron microscopy with a FEI-Q FEG250 system. The optical properties of the samples were obtained by UV-Vis diffuse reflectance spectroscopy (DRS, Lambda-950) in the wavelength of 300-800 nm. Steady-state photoluminescence was performed on an Edinburgh FLS980 with an excitation wavelength of 385 nm. Time-resolved PL spectra were recorded on a Leica DMi8 system with a pulsed white light laser (SuperK Extreme EXW-12, NKT Photonics) operating at 405 nm. X-ray photoelectron spectroscopy measurements were performed using a monochromatized Al Kα X-ray source, and the C 1s signal was set to a position of 284.6 eV. Photoelectrochemical measurements were performed with a standard three-electrode setup by using Ag/AgCl and platinum sheet electrode as the reference electrode, and counter electrode, respectively. Targeted material deposited on an indium tin oxide (ITO) substrate serves as the working electrode. Dichloromethane (DCM) solution containing 0.1 M tetrabutylammonium hexafluorophosphate ($TBAPF_6$) was used as the electrolyte. Photocurrent response measurements were performed under simulated solar light irradiation. Electrochemical impedance spectroscopy (EIS) was recorded at a frequency of 10 KHz-5 MHz under 0.2 V open circuit potential. Mott-Schottky measurements were performed in the dark at a frequency of 1 KHz. Surface charge transfer efficiency (η_t) of the materials was carried out using methylviologen dichloride ($MVCl_2$) as a fast electron scavenger.[2, 3]

3.2 Density functional theory (DFT) calculations

Density functional theory (DFT) calculations were performed by the *Vienna ab initio* simulation package (VASP). The Perdew-Burke-Ernzerh (PBE) function is used for structural optimization and charge density. The plane waves cutoff energy is 400 eV. A mesh of 4×4×4 and 6×6×6 k-points was adopted for structural optimization and electronic calculation. The convergence tolerance of energy and the force are 1×10^{-4} eV and 1×10^{-2} eV/Å, respectively.

The carrier effective mass is simulated by the band edges of the band gap which can

be expressed by this formula:

$$m^* = \hbar^2 \frac{\partial \varepsilon^2 (k)}{\partial k^2}^{-1} \quad (1)$$

where *k* is the wave vector, *ε(k)* represents the eigenvalues of the energy band, and $\hbar$ is reduced Planck's constant. In this work, we calculate the average effective mass in Γ point from X- Γ-Y in xy plane. The selected K-point coordinates are X (0.5 0 0), Y (0 0.5 0), and Γ (0 0 0). To ensure the accuracy of the calculation, we insert 80 k-points from X-Γ (X-vector direction) and Γ-Y (Y-vector direction).

The carrier mobility formula is

$$\mu_{3D} = \frac{(8\pi)^{\frac{1}{2}} \hbar^4 e c_{ii}}{3(m*)^{\frac{5}{2}} (k_B T)^{\frac{3}{2}} {E_1}^2} \quad (2)$$

where C_{ii} is 3D elastic constants, E_1 is the deformation potential: $E_1 = \Delta E/(\Delta l/l_0)$, E is the energy of conduction (valence) band edges, l_0 is optimized lattice constants, e is the elementary charge, $\hbar$ is reduced Planck's constant, and K_B is Boltzmann constant.

3.3 Photocatalytic activity evaluation

Photocatalytic reactions were conducted in a 25 mL quartz reactor under simulated solar light illumination (150 W Xe lamp). More specifically, 15 mg photocatalyst and 0.1 mmol benzyl alcohol (BA) were added to 2.5 mL benzotrifluoride with saturated molecular oxygen. Then, the mixture was irradiated for 6 h under magnetic stirring (600 rpm). Finally, the mixture was centrifuged, and the liquid was analyzed by GC (Shimadzu 2010). The conversion and selectivity of BA were defined as follows:

Conversion (%) = $[(C_0\text{-}C_A)/C_0] \times 100\%$

Selectivity (%) = $[C_B/(C_0\text{-}C_A)] \times 100\%$

Where C_0 is the initial concentration of BA, C_A and C_B are the concentrations of the BA and benzaldehyde (BAD) after the reaction, respectively.

4. Main text supporting characterization

Table S1. Calculated lattice parameters (a, b, c, α, β, γ) for $Cs_3Bi_2Br_9$ and Cs_3BiBr_6.

Parameter	$Cs_3Bi_2Br_9$	Cs_3BiBr_6
a (Å)	8.21	8.80
b (Å)	8.21	14.11
c (Å)	10.07	28.30
α (◦)	90	90
β (◦)	90	90
γ (◦)	120	100.33

Table S2. Bond lengths (Å) and angles (deg) for $Cs_3Bi_2Br_9$ and Cs_3BiBr_6 compounds.

$Cs_3Bi_2Br_9$	Bond lengths (Å)	Bi-Br1	3.02529(0)
		Bi-Br2	2.75916(0)
	Angles (deg.)	Br1-Bi-Br2 (#1)	174.5991(0)
		Br1-Bi-Br1	85.5220(0)
		Br2-Bi-Br2	93.1931(0)
		Br1-Bi-Br2 (#3)	90.5166(0)
Cs_3BiBr_6	Bond lengths (Å)	Bi1-Br2	2.83499(0)
		Bi1-Br3	2.86845(0)
		Bi1-Br5	2.86144(0)
		Bi1-Br6	2.85746(0)
		Bi2-Br1	2.84724(0)
		Bi2-Br4	2.86583(0)
		Bi1-Br7	2.82263(0)
	Angles (deg.)	Br2-Bi1-Br2	93.8893(0)
		Br2-Bi1-Br3 (#1)	84.1987(0)
		Br2-Bi1-Br5	90.6999(0)
		Br2-Bi1-Br6	90.7180(0)
		Br2-Bi1-Br3 (#3)	178.0859(0)
		Br1-Bi2-Br1	89.9542(0)
		Br1-Bi2-Br4 (#1)	92.6560(0)
		Br1-Bi2-Br7 (#1)	90.1820(0)
		Br1-Bi2-Br4 (#3)	176.5204(0)
		Br1-Bi2-Br7 (#2)	87.8212(0)
		Br4-Bi2-Br4	84.8307(0)
		Br7-Bi2-Br7	177.1777(0)

#n (n=1, 2, 3) represents the number of adjacent atoms.

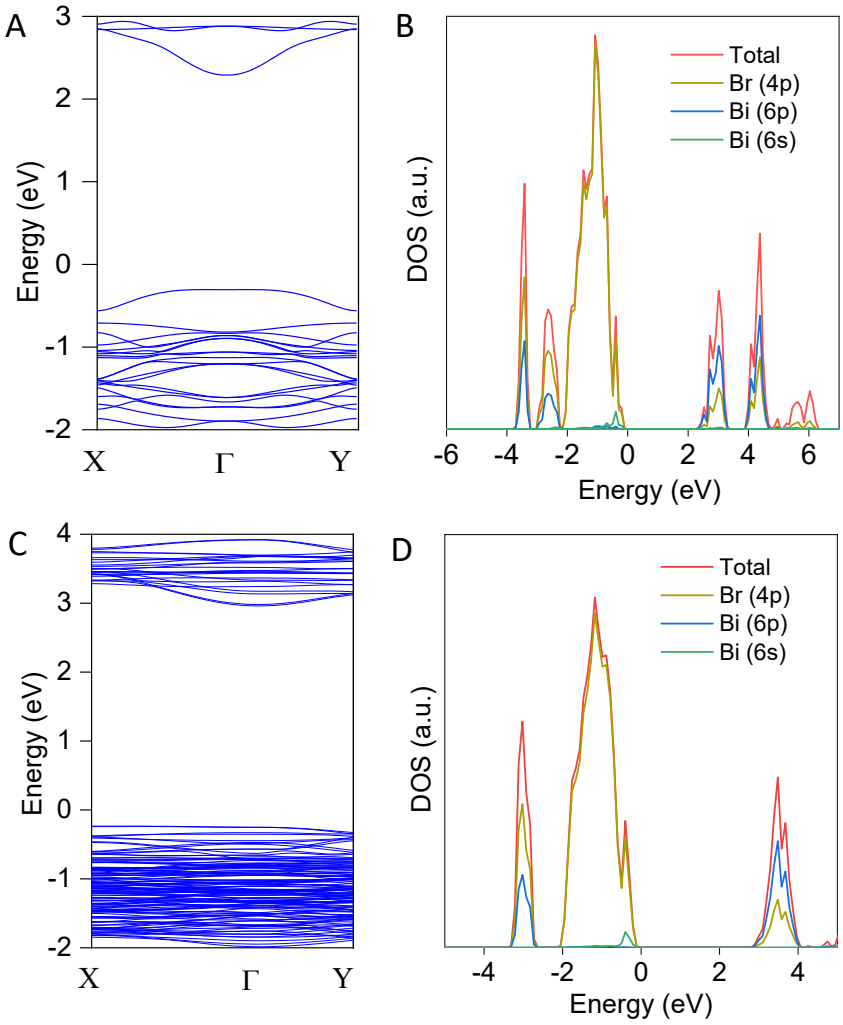

Fig. S1. The band structure and density of states (DOS) of (A and B) $Cs_3Bi_2Br_9$ and (C and D) Cs_3BiBr_6, respectively, where the selected K-point coordinates are X (0.5 0 0), Y (0 0.5 0), and Γ (0 0 0).

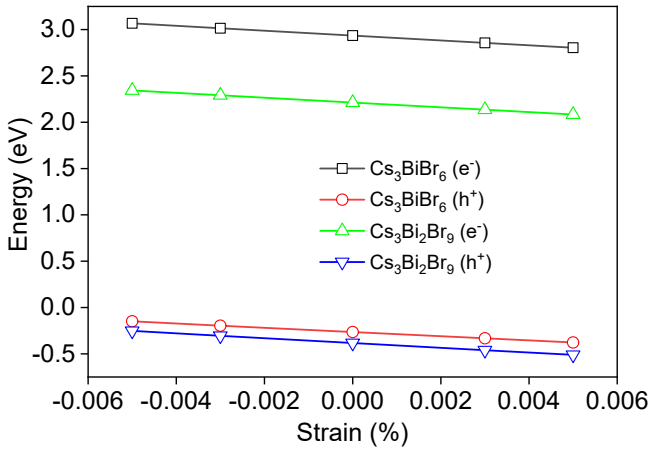

Fig. S2. Shifts of the conduction band and valence band under uniaxial strain. The deformation potential constants (the slope of the fitting lines) of $Cs_3Bi_2Br_9$ and Cs_3BiBr_6 are different, which is consistent with the results of carrier effective masses and carrier mobility (μ).

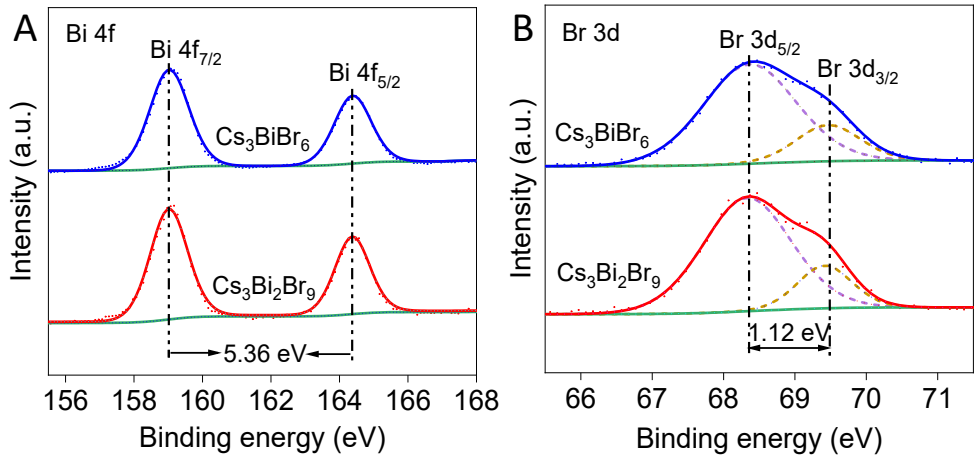

Fig. S3. High-resolution XPS spectra of (A) Bi 4f and (B) Br 3d core levels.

Table S3. Atomic ratios of $Cs_3Bi_2Br_9$ and Cs_3BiBr_6 deduced from XPS analysis.

Element		Cs		Bi		Br	
Core level		Cs $3d_{5/2}$	Cs $3d_{3/2}$	Bi $4f_{7/2}$	Bi $4f_{5/2}$	Br $3d_{5/2}$	Br $3d_{3/2}$
Relative Sensitivity Factor (RSF)		23.76	16.46	13.90	10.93	1.68	1.16
$Cs_3Bi_2Br_9$	Area	12600.2	7970.8	6015.6	3419.2	3097.1	1469.9
	Atom ratio	Cs:Bi:Br=3:2.21:9.20					
Cs_3BiBr_6	Area	11711.2	8275.3	2849.0	2190.6	2136.1	978.3
	Atom ratio	Cs:Bi:Br=3:1.22:6.37					

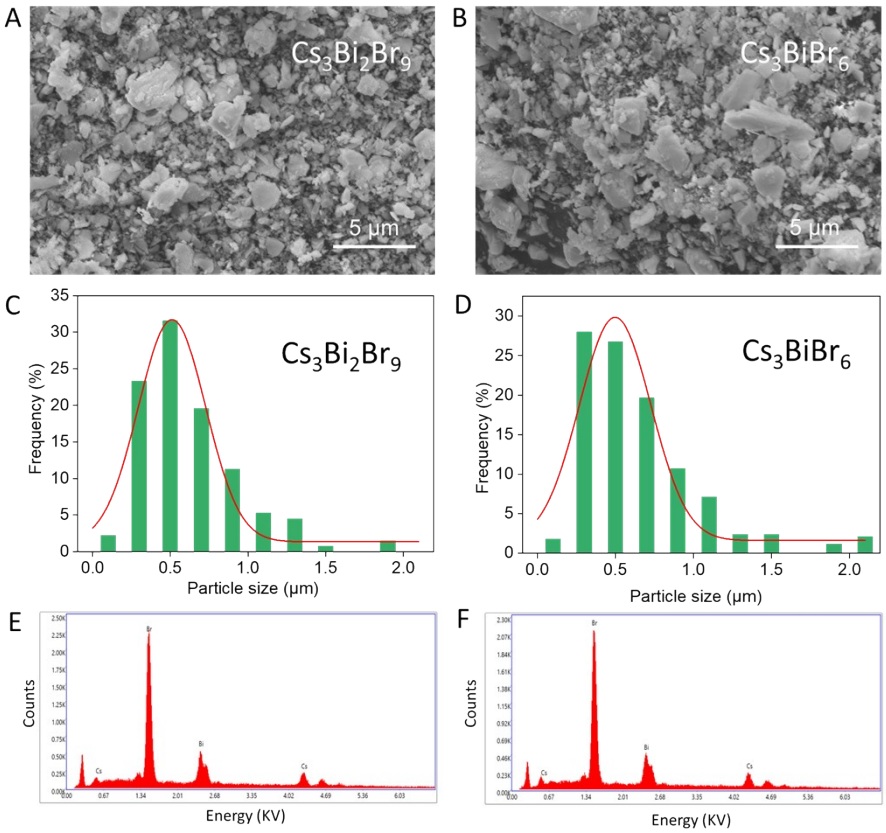

Fig. S4. (A-B) SEM images of (A) $Cs_3Bi_2Br_9$ and (B) Cs_3BiBr_6 materials. (C-D) Particle size distribution (C) $Cs_3Bi_2Br_9$ and (D) Cs_3BiBr_6. (E-F) EDS spectra recorded for (E) $Cs_3Bi_2Br_9$ and (F) Cs_3BiBr_6.

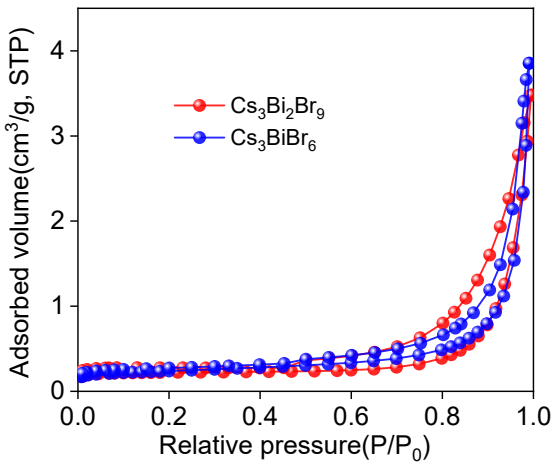

Fig. S5. Nitrogen adsorption-desorption isotherms of $Cs_3Bi_2Br_9$ and Cs_3BiBr_6 materials.

Table S4. BET surface areas, pore size and pore volume of $Cs_3Bi_2Br_9$ and Cs_3BiBr_6 samples.

Material	SBET (m^2/g)	pore size (nm)	pore volume (cm^3/g)
$Cs_3Bi_2Br_9$	1.53	2.13	0.017
Cs_3BiBr_6	1.47	2.05	0.016

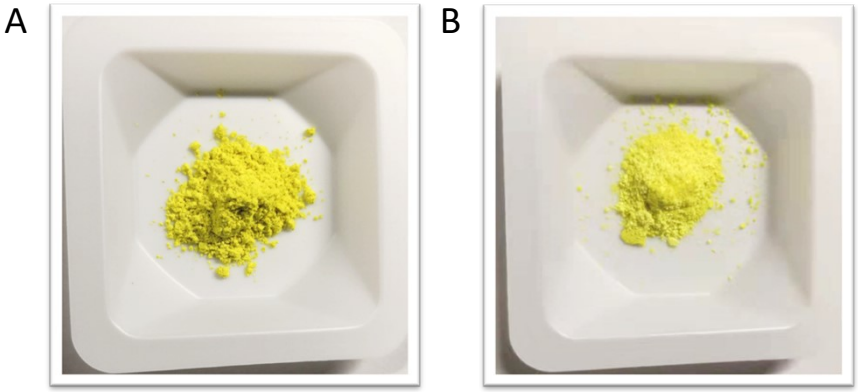

Fig. S6. The digital photographs of (A) $Cs_3Bi_2Br_9$ and (B) Cs_3BiBr_6 materials.

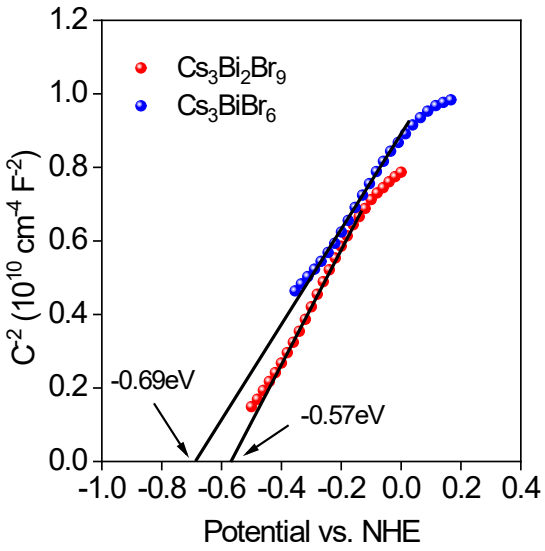

Fig. S7. Mott-Schottky plots of $Cs_3Bi_2Br_9$ and Cs_3BiBr_6.

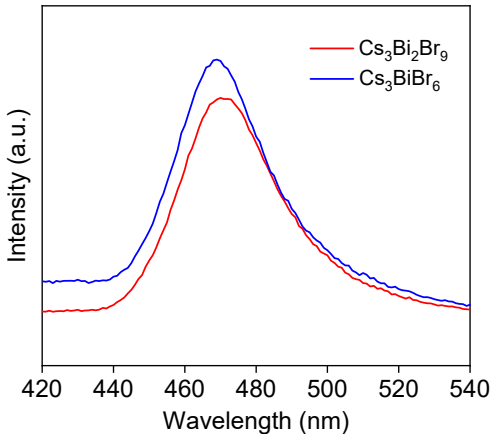

Fig. S8. Steady-state PL spectra of $Cs_3Bi_2Br_9$ and Cs_3BiBr_6 materials.

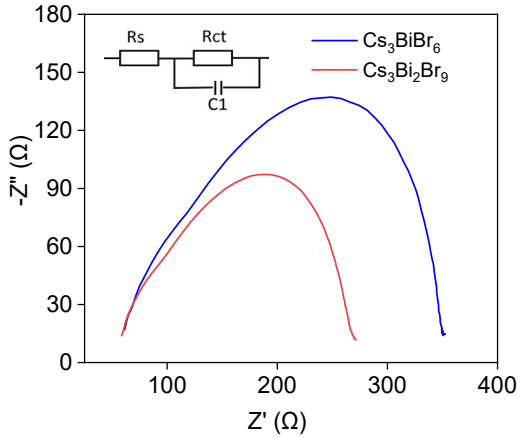

Fig. S9. EIS Nyquist plots of $Cs_3Bi_2Br_9$ and Cs_3BiBr_6 materials.

Table S5. Comparison of Selective Photocatalytic Oxidation of Benzyl Alcohol (BA) to Benzaldehyde (BAD) over MHP-based and Other Photocatalysts.

Catalyst	Light source	Solvent	T (°C)	Conversion (%)	Selectivity (%)	Production rate (mmol g^{-1} h^{-1})	Ref.

$Cs_3Bi_2Br_9$ /TiO_2	Xe lamp (150W, >420 nm)	Toluene	25	73	97.7	0.91	[4]
$Cs_3Sb_2Br_9$	Xe lamp (150W, AM1.5G)	Toluene	70	47	83	0.29	[5]
$CsPbBr_3/TiO_2$	Xe lamp (300W, >420 nm)	Toluene	80	50	90	0.5	[6]
$FAPbBr_3$/ TiO_2	Xe lamp (150W, AM1.5G)	Toluene	25	63	99	0.8	[7]
$CsPbX_3$/ $W_{18}O_{49}$	Xe lamp (150W, AM1.5G)	Hexene	25	72	>99	1.5	[8]
$NiO_x/FAPbBr_3$ /TiO_2	Xe lamp (150W, AM1.5G)	Toluene	25	/	/	3.8	[9]
TiO_2/CeO_2	Xe lamp (300W, >420 nm)	H_2O	25	34	39	0.006	[10]
Cu@NALC/ TiO_2/AC	Xe lamp (100 mW/cm^2)	MeCN	25	100	>99	0.02	[11]
F-WO_3	Xe lamp (500W, 320-780 nm)	H_2O	25	57	99	0.04	[12]
Bi-TATB MOF	Xe lamp (300W)	Hexene	15	38	100	0.08	[13]
CdS/g-C_3N_4	Xe lamp (300W, >420 nm)	Benzotrifluoride	60	48	99	0.4	[14]
g-C_3N_4	Xe lamp (300W, >420 nm)	Benzotrifluoride	100	23	98	1.2	[15]
g-C_3N_4/ $W_{18}O_{49}$	Xe lamp (500W, 320-780 nm)	H_2O	25	40	99.8	2.2	[16]
CdS@MoS_2	Xe lamp (300 W, >420 nm)	MeCN	25	95	99	2.3	[17]
$Cs_3Bi_2Br_9$/Pd	Xe lamp (150W, AM1.5G)	Benzotrifluoride	25	82.3	>99	9.1	**This work**

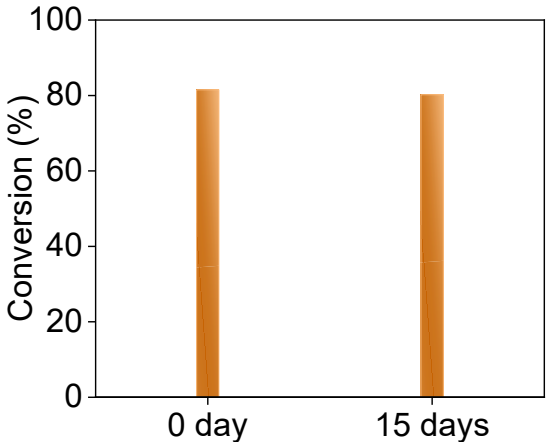

Fig. S10. Stability test of Pd/$Cs_3Bi_2Br_9$ composite after exposure to air for 15 days.

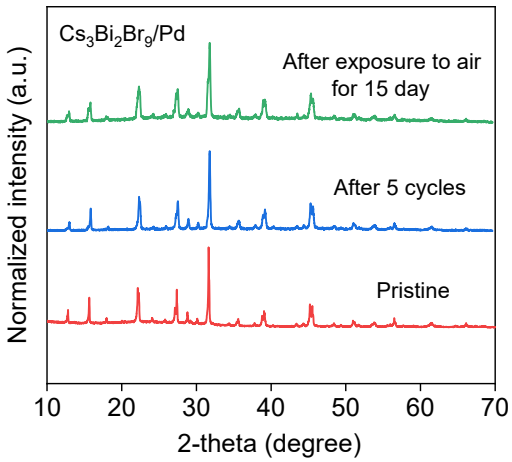

Fig. S11. XRD patterns of $Cs_3Bi_2Br_9$/Pd composite before and after 5 cycles and exposed to air for 15 days.

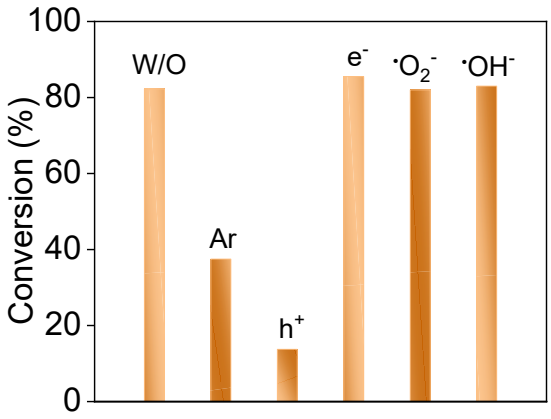

Fig. 12. Effects of radical scavengers on the photocatalytic performance of BA oxidation over $Cs_3Bi_2Br_9$/Pd composite, where W/O means without scavengers, Ar represents the oxygen is replaced by argon gas, e^-, h^+, $^{\bullet}O_2^-$ and $^{\bullet}OH^-$ denote the reaction system with potassium persulfate, ammonium oxalate, 1,4-benzoquinone and t-butanol additives, respectively. Reaction conditions: 0.1 mmol BA in 2.5 mL molecular oxygen saturated benzotrifluoride, 15 mg catalyst, simulated solar light (AM 1.5G, 150 W Xe lamp), reaction time (6 h).

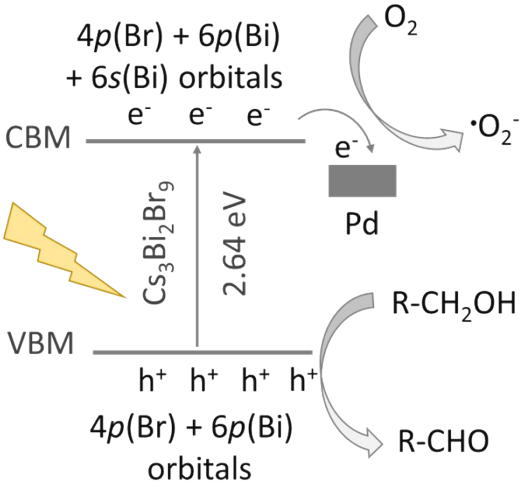

Fig. S13. Schematic illustration of the photocatalytic BA oxidation over Pd/$Cs_3Bi_2Br_9$ photocatalyst.

Scheme S1. The proposed reaction equations for the photocatalytic oxidation of BA to BAD over Pd/$Cs_3Bi_2Br_9$ composite.

$$Cs_3Bi_2Br_9 + hv \rightarrow h^+ + e^- \quad (1)$$

$$O_2 + e^- \rightarrow {}^{\bullet}O_2^- \quad (2)$$

$$C_6H_5CH_2OH + h^+ \rightarrow C_6H_5CHOH{\bullet}^* + H^+ \quad (3)$$

$$C_6H_5CHOH{\bullet}^* + h^+ \rightarrow C_6H_5CHO + H^+ \quad (4)$$

$$2\ H^+ + 2\ {}^{\bullet}O_2^- \rightarrow H_2O + 3/2\ O_2 \quad (5)$$

5. References

1 B. Weng, Q. Quan and Y.-J. Xu, *J. Mater. Chem.A*, 2016, **4**, 18366-18377.

2 C. Feng, L. Tang, Y. Deng, J. Wang, Y. Liu, X. Ouyang, H. Yang, J. Yu and J. Wang, *Appl. Catal. B: Environ.*, 2021, **281**, 119539.

3 C. Feng, L. Tang, Y. Deng, J. Wang, J. Luo, Y. Liu, X. Ouyang, H. Yang, J. Yu and J. Wang, *Adv. Funct. Mater.*, 2020, **30**, 2001922.

4 Q. Sun, W. Ye, J. Wei, L. Li, J. Wang, J.-H. He and J.-M. Lu, *J. Alloys Compd.*, 2022, **893**, 162326.

4 D. Wu, W. Sang, B. Huo, J. Wang, X. Wang, C. Chen, Q. Huang and X. Tang, *J. Catal.*, 2022, **408**, 36-42.

6 S. Schünemann, M. van Gastel and H. Tüysüz, *ChemSusChem*, 2018, **11**, 2057-2061.

7 H. Huang, H. Yuan, K. P. F. Janssen, G. Solís-Fernández, Y. Wang, C. Y. X. Tan, D. Jonckheere, E. Debroye, J. Long, J. Hendrix, J. Hofkens, J. A. Steele and M. B. J. Roeffaers, *ACS Energy Lett.,* 2018, **3**, 755-759.

8 R. Cheng, J. A. Steele, M. B. Roeffaers, J. Hofkens and E. Debroye, *ACS Appl. Energy Mater.*, 2021, **4**, 3460-3468.

9 H. Huang, H. Yuan, J. Zhao, G. Solís-Fernández, C. Zhou, J. W. Seo, J. Hendrix, E. Debroye, J. A. Steele, J. Hofkens, J. Long and M. B. J. Roeffaers, *ACS Energy Lett.*, 2018, **4**, 203-208.

10 S. Li, J. Cai, X. Wu, B. Liu, Q. Chen, Y. Li and F. Zheng, *J. Hazard. Mater.*, 2018, **346**, 52-61.

11 M. Farrag and R. Yahya, *J. Photochem. Photobiol. A: Chem.*, 2020, **396**, 112527.

12 Y. Su, Z. Han, L. Zhang, W. Wang, M. Duan, X. Li, Y. Zheng, Y. Wang and X. Lei,

Appl. Catal. B: Environ., 2017, **217**, 108-114.

13 R. Zhang, Y. Liu, Z. Wang, P. Wang, Z. Zheng, X. Qin, X. Zhang, Y. Dai, M.-H. Whangbo and B. Huang, *Appl. Catal. B: Environ.*, 2019, **254**, 463-470.

14 X. Dai, M. Xie, S. Meng, X. Fu and S. Chen, *Appl. Catal. B: Environ.*, 2014, **158**, 382-390.

15 L. Zhang, D. Liu, J. Guan, X. Chen, X. Guo, F. Zhao, T. Hou and X. Mu, *Mater. Res. Bull.*, 2014, **59**, 84-92.

16 C. Xiao, L. Zhang, H. Hao and W. Wang, *ACS Sustain. Chem. Eng.*, 2019, **7**, 7268-7276.

17 P. Li, H. Zhao, X. Yan, X. Yang, J. Li, S. Gao and R. Cao, *Sci. China Mater.*, 2020, **63**, 2239-2250.